NUMERICAL MODELING OF COLD SWAGING OF SINTERED W-BASED ALLOY

DOHNALÍK Daniel[1], BAGHIROVA Banovsha[1], HAJÍČEK Michal[2], FUSEK Martin[3], KUBÍN Tomáš[3]

[1]Faculty of Metallurgy and Materials Engineering, VSB - Technical University Ostrava, Czech Republic, EU
[2] UJP PRAHA a.s., Prague, Czech Republic, EU
[3]Faculty of Mechanical Engineering, VSB - Technical University Ostrava, Ostrava, Czech Republic, EU

Abstract

This paper numerically and experimentally describes the influence of cold rotary swaging on a pre-sintered tungsten alloy. The finite element method was applied to describe infeed swaging of 30 mm diameter circular bar with 30% reduction of cross-sectional area. The numerically studied results were distribution of strain, distribution of temperature, effective strain rate and material flow during a single pass. To validate the predicted results, experimental swaging of pre-sintered W-Ni-Co tungsten alloy was realized. The results of strain distribution were compared with results from microstructure analysis and distribution of microhardness along the cross section of the swaged sample. Results of mechanical testing showed higher microhardness in regions near the swaged surface. This fact corresponds to the distribution of strain predicted by numerical modeling

Keywords: Numerical modeling, cold swaging, tungsten alloy

1. INTRODUCTION

Rotary swaging is a metal forming process for reducing of cross-sections of bars, tubes and wires via imposing of intensive plastic deformation. It is suitable for various materials including materials with low formability due to predominantly compressive stresses [1, 2]. The principle of the technology is in an oscillating movement of tools, during which the strain is imposed into the material in many small increments. Rotary swaging features inhomogeneity of deformation along the cross section, since the imposed strain is the highest near the surface of the sample, especially for low imposed strains. Deformation (in)homogeneity along the cross section can be evaluated e.g. by microhardness testing [3, 4]. However, a certain inhomogeneity of the imposed strain for relatively small overall strains is characteristic for many processes imposing intensive plastic deformation into materials, such as methods of severe plastic deformation (e.g. HPT [5], ECAP [6], TE [7], ARB [8] etc.).

Swaging is often used also for pre-sintered tungsten-based alloys prepared using powder metallurgy. Tungsten-based alloys usually consist of more or less spherical tungsten grains and a matrix between the grains [9]. For example, tungsten-based alloys of W-Ni-Co type after sintering and heat treatment achieve up to 20% elongation and 800-1000 MPa ultimate strength [10-12]. The degree of elongation and strength properties are primarily dependent on the amount of matrix in the particular structure [10]. However, maximum elongation decreases and strength increases after cold forming due to strain hardening.

The aim of this work is to perform a numerical modelling of rotary swaging process for tungsten-based alloy under cold conditions. The predicted results, especially the distribution of strain, are subsequently evaluated experimentally. The effect of swaging is evaluated by microhardness measurements and microstructure observations.

2. EXPERIMENTAL

For numerical and also experimental swaging of the bar, four dies are used (**Figure 1a**). A swaging die is composed of three zones, reduction, calibration and exit zone (**Figure 1b**). During the process, all the dies rotate around the swaging axis after each blow. A manipulator was used for feeding of the workpiece into the

swaging head; the workpiece was fed to the swaging head when the dies were open. Forging was carried out at room temperature, temperature of the workpiece and dies was set to 20 °C. Friction between the dies and workpiece was determined via the Coulomb law with the friction coefficient of μ = 0.1. Initial dimensions of the sample were the diameter of 30 mm and length of 100 mm, the final diameter of the swaged sample was 25 mm and the true strain imposed during the single pass was 0.36.

To describe the flow stress of the 91W-6Ni-3Co pre-sintered alloy, a mathematical model based on stress-strain curve obtained using a tensile test performed on the experimentally swaged alloy was used. Material for cold swaging was prepared using the technology of powder metallurgy. Its fabrication involved several steps. These are mixing of metal powders, cold isostatic pressing (pressure of 400 MPa) and high temperature sintering (1540 °C) for many hours. Experimental swaging was carried out at room temperature. To determine the effect of swaging on mechanical properties, samples for analyses were prepared by grinding on SiC papers and mechanical polishing and subsequently subjected to HV0.1 Vickers microhardness measurements and microstructure scanning using a Quanta FEG 450 SEM scanning electron microscope.

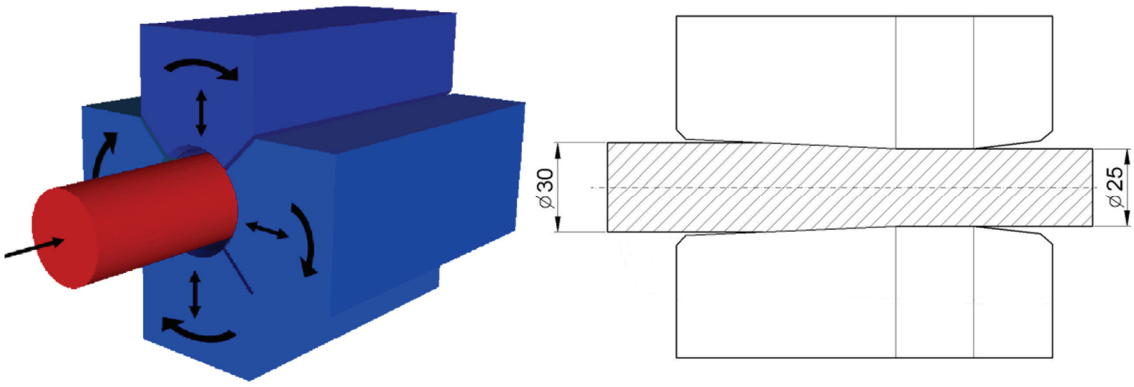

Figure 1 (a) Geometry of the assembly; (b) Geometry of a die

3. RESULTS AND DISSCUSION

3.1. Effective strain

The distribution of the effective strain in the longitudinal cross section during swaging shows **Figure 2a**. During a pass, the effective strain increases in the reduction zone, while in the calibration zone the effective strain achieves its final values. The effective strain is higher on the surface, but the effect of deformation can be seen in the central region, too.

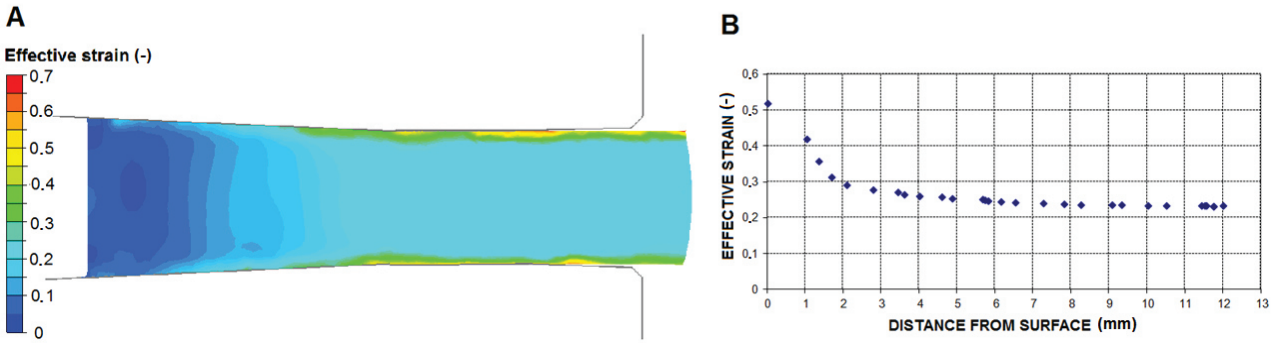

Figure 2 (a) Effective strain across the central cutting plane; (b) dependence of effective strain on distance from the surface

Figure 2b shows the distribution of the effective strain related to the distance from the swaged surface. In the distance of 2 mm from the surface, the strain is significantly higher, while from the distance of 2 mm towards the axis of the sample, the strain is more or less homogenous. Another swaging experiment published by others [13] reported a significantly higher strain in the near-surface area after one swaging pass. For the reduction of the diameter from 8 mm to 7 mm (true strain of 0.26), the equivalent strain in the center was 0.25 and in the surface area it was 0.45; while for the reduction from 8 mm to 6.6 mm (true strain of 0.38), the effective strain in the center was 0.3 and in the surface area it was 0.7. The values of the effective strain for the true strain of 0.38 reported by Rong et al. [13] are comparable to the values predicted in this numerical simulation for the true strain of 0.36. Mourni et al. [3] documented that swaging with a higher reduction from the diameter of 1 mm to 0.5 mm (true strain of 1.38) was characterized by inhomogeneous strain, the equivalent strain on the surface was 1.55 and in the center it was 1.4. A comparison of the distribution of strain for the presented experiment and swaging with a higher total strain (1.38) shows decreasing strain inhomogeneity with increasing imposed strain. It can be supposed that increasing imposed strain (i.e. swaging in multiple passes) would result, for our tungsten-based alloy, in homogenization of the strain across the cross section, having the value close to the values predicted for the surface areas after the first pass.

3.2. Temperature and strain rate

Temperature and strain rate distributions in the central longitudinal cross section are shown in **Figure 3**. During the swaging process heat generates as a result of plastic deformation and friction. The initial temperature of the sample was 20 °C and during swaging it increased to the maximum value of approximately 70 °C. Areas with maximum temperature were localized at the interface between the reduction and calibration zones, near the swaged surface. Significantly higher values of strain rate were in the reduction zone near the surface, where the most significant amount of strain was imposed. The maximum value of strain rate was approximately 5 s^{-1}. When compared to other forming technologies, the strain rate was quite low since, during swaging, single blows were characterized by a low deformation degree.

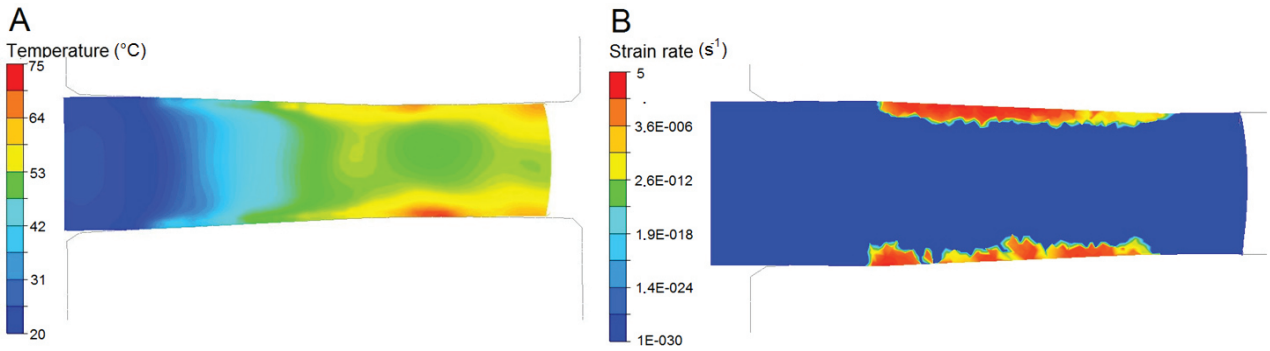

Figure 3 (a) Temperature; (b) strain rate in central cutting plane

3.3. Swaging force

The force during swaging depends mainly on the flow stress of material, velocity of feeding, friction coefficient and size of the contact surface between the dies and sample. Evolution of force during a pass is shown in **Figure 4**, in which each of the peaks corresponds to a single blow. The force was measured for one die along Y axis. Due to rotation of the dies, the axis of the die changes in the coordinate system and the values of the force correspond to reality in every sixth blow (axis of the die corresponds to Y axis). The dependence in **Figure 4** shows that the force depends on the contact surface. The force reaches its maximum when the sample fills the whole reduction zone and calibration zone. The maximum value of the force is approximately 700 kN.

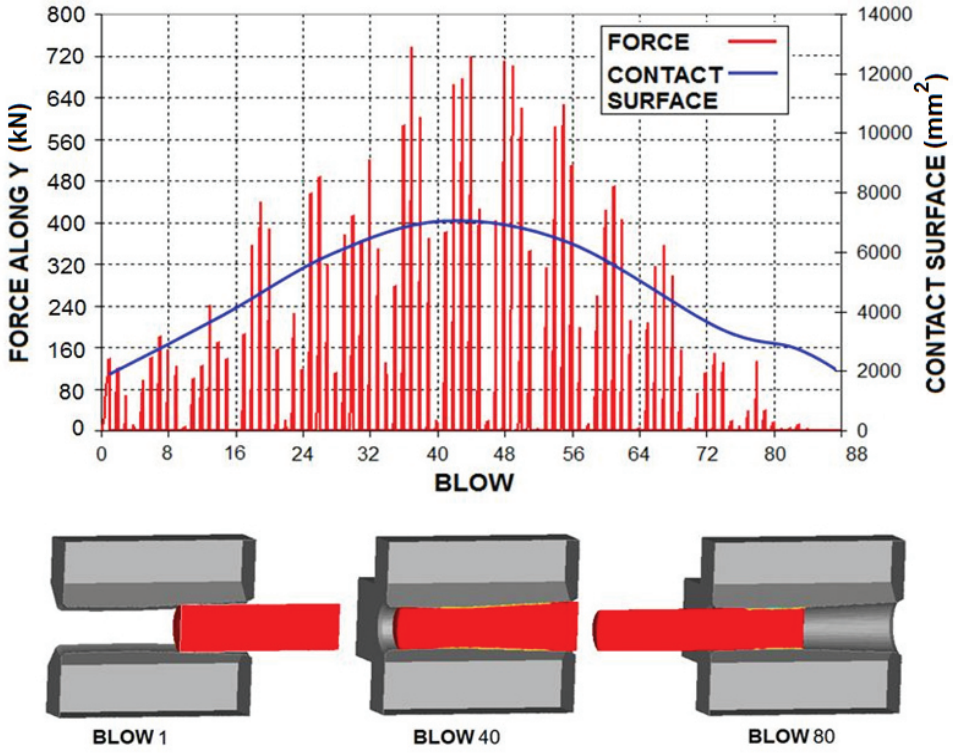

Figure 4 Prediction of force

3.4. Material flow

Material flow during swaging is depicted in **Figure 5a**. Material flow is evaluated in relation with the displacement along Z axis. The displacement increases in the reduction zone due to reducing cross section. In the calibration zone, the displacement is constant having the value of ~ 0.5 mm. **Figure 5b** describes material flow using a grid consisting of 1 x 1 mm squares.

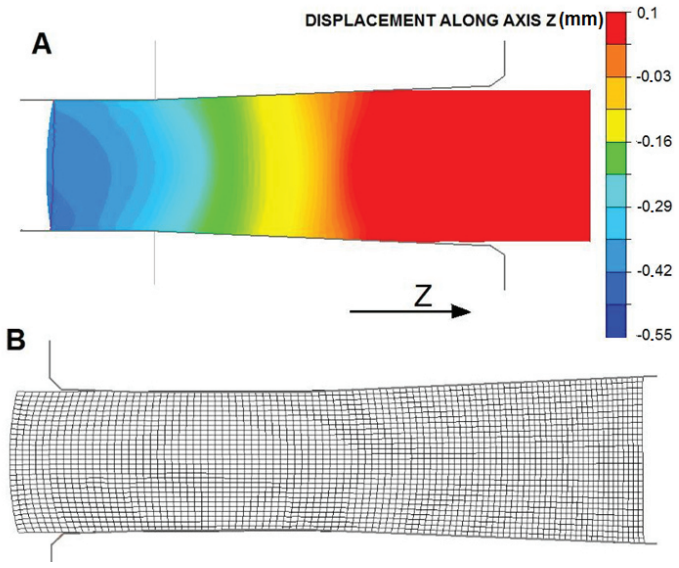

Figure 5 (a), (b) material flow

3.5. Experimental verification

Deformation under cold conditions is characterized by strain hardening; hardness and strength of material depend on the amount of imposed strain. **Figure 6** shows a comparison of experimentally measured microhardness and effective strain resulting from the numerical simulation in the cross section of the sample. Since the experimental alloy consists of tungsten grains and a matrix, measurement of micro-hardness was performed for both the phases. Microhardness of both the phases increases in the direction from the center towards the surface. However, the effect of strain hardening is more significant for tungsten grains, while hardening of the matrix is not so substantial.

The effect of swaging can also be observed on images of microstructure (**Figure 7**). The alloy after sintering consists of spherical grains of tungsten and a matrix. The structure of pre-sintered tungsten-based alloys after swaging is typically characterized by elongated tungsten grains (the degree of elongation depends on the reduction of the cross-sectional area) [14]. However, in the central region tungsten grains can still be spherical, especially when only a low reduction is applied [4]. **Figure 7** shows a comparison of structures from the central and surface areas after swaging. Due to inhomogeneous strain, more elongated grains can be seen near the surface of the sample. **Figure 7c** shows the structure from the central area, where the grains are also elongated, although less than in the peripheral regions.

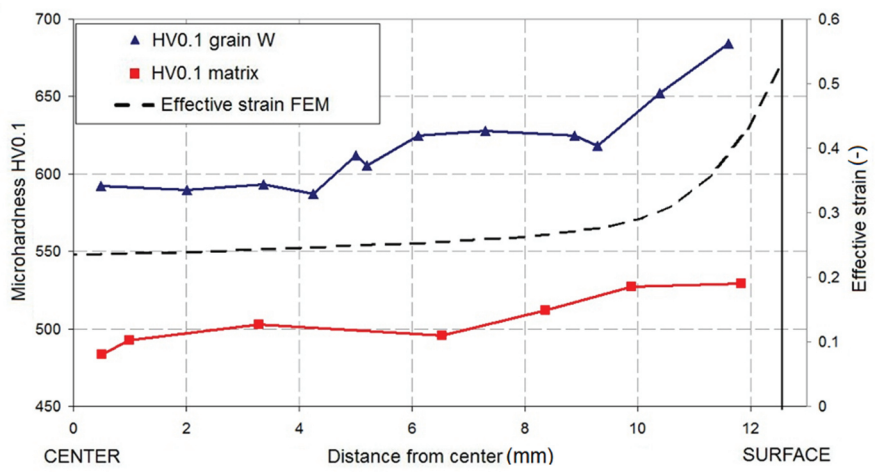

Figure 6 Measured microhardness after swaging

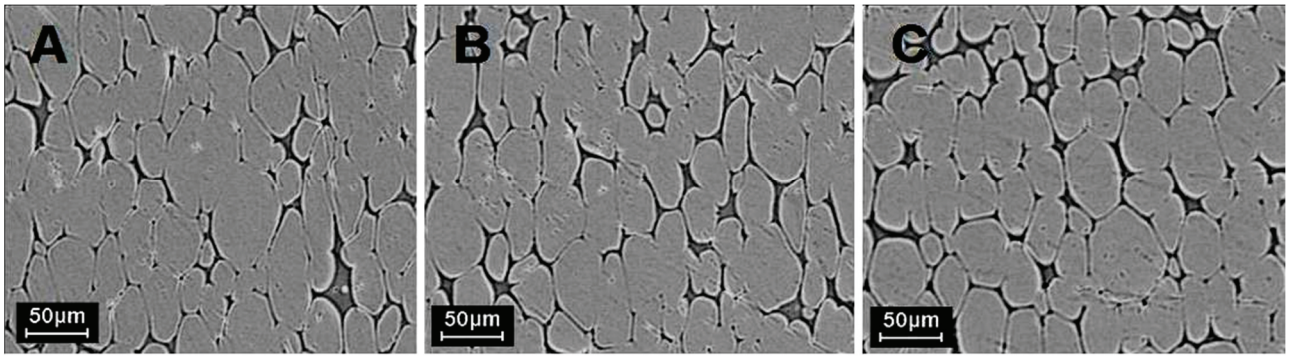

Figure 7 Microstructure of swaged sample; (a) surface; (b) between centre and surface; (c) central region

4. CONCLUSION

The FEM analysis performed within this study describes distribution of effective strain within a swaged sample. The results show inhomogeneity of strain along the cross section, the strain increases in the direction from the axis towards the surface. Significantly higher values of strain are at the area located 2 mm from the surface. The maximum swaging force was detected when the sample fills the reduction and calibration zones, in which the force increases to approximately 700 kN. To verify the distribution of effective strain, microhardness of the swaged sample was compared with the FEM results. The microhardness along the cross section corresponds to distribution of effective strain (FEM), microhardness of the individual phases increases towards the surface. Significant hardening exhibited especially tungsten grains, microhardness HV0.1 was in centre 595 and near the surface 690. Microstructure images show the tungsten grains to be more elongated at peripheral areas due to a higher strain imposed into the surface area.

ACKNOWLEDGEMENTS

This paper was created within the research project no. SP2016/66 and funded by INFINITY project in the framework of the EU Erasmus Mundus Action 2.

REFERENCES

[1] KOCICH, R., MACHÁČKOVÁ, A., KUNČICKÁ, L., FOJTÍK, F. Fabrication and characterization of cold-swaged multilayered Al-Cu clad composites. *Materials & Design*, 2015, vol. 71, pp. 36-47.

[2] KOCICH, R., KUNČICKÁ, L., DAVIS, C. F., LOWE, T. C., SZURMAN, I., MACHÁČKOVÁ, A. Deformation behavior of multilayered Al-Cu clad composite during cold-swaging. *Materials & Design*, 2016, vol. 90, pp. 379-388.

[3] MOUMI, E. et al. 2D-simulation of material flow during infeed rotary swaging using finite element method. *Procedia Engineering*, 2014, vol. 81, pp. 2342 -2347.

[4] KATAVIĆ, B., NIKAČEVIĆ, M., ODANOVIĆ, Z. Effect of cold swaging and heat treatment on properties of the P/M 91W-6Ni-3Co heavy alloy. *Science of Sintering*, 2008, vol. 40, pp. 319-331.

[5] KUNČICKÁ, L., LOWE, T. C., DAVIS, C. F., KOCICH, R., POHLUDKA, M. Synthesis of an Al/Al_2O_3 composite by severe plastic deformation. *Materials Science and Engineering A*, 2015, vol. 646, pp. 234-241

[6] KOCICH, R., GREGER, M., MACHÁČKOVÁ, A. finite element investigation of influence of selected factors on ECAP process. In *METAL 2010: 19th International Metallurgical and Materials Conference*. Ostrava: TANGER, 2010. pp. 166-171.

[7] NOOR, S. V., EIVANI, A. R., JAFARIAN, H.R., MIRZAEI, M. Inhomogeneity in microstructure and mechanical properties during twist extrusion. *Materials Science and Engineering A*, 2016, vol. 652, pp. 186-191.

[8] KOCICH, R., MACHÁČKOVÁ, A., FOJTÍK, F. Comparison of strain and stress conditions in conventional and ARB rolling processes. *International Journal of Mechanical Sciences*, 2012, vol. 64, no. 1, pp. 54-61.

[9] DINÇER, O., et al. Processing and microstructural characterization of liquid phase sintered tungsten-nickel-cobalt heavy alloys. *International Journal of Refractory Metals and Hard Materials*, 2015, vol. 50, pp. 106-112.

[10] KIRAN, U. R., et al. Effect of tungsten content on microstructure and mechanical properties of swaged tungsten heavy alloys. *Materials Science & Engineering A*, 2013, vol. 582, pp. 389-396.

[11] KIRAN, U. R., et al. Swaging and heat treatment studies on sintered 90W-6Ni-2Fe-2Co tungsten heavy alloy. *International Journal of Refractory Metals and Hard Materials,* 2012, vol. 33, pp.113-121.

[12] DAS, J., et al. Thermo-mechanical processing, microstructure and tensile properties of a tungsten heavy alloy. *Materials Science & Engineering A*, 2014, vol. 613, pp.48-59.

[13] LI, R., ZUO-REN, N., TIE-YONG, Z. FEA modelling of effect of axial feeding velocity on strain field of rotary swaging process of pure magnesium. *Transactions of Nonferrous Metals Society of China*, 2006, vol. 16, no. 5, pp.1015-1020.

[14] YU, Z., ZHANG, W., CHEN, Y., Wang, E. Effect of swaging on microstructure and mechanical properties of liquid-phase sintered 93W-4.9(Ni, Co)-2.1Fe alloy. *International Journal of Refractory Metals and Hard Materials*, 2014, vol. 44, pp. 103-108.